MATERIALS CHEMISTRY FRONTIERS

CHINESE CHEMICAL SOCIETY

ROYAL SOCIETY OF CHEMISTRY

RESEARCH ARTICLE

View Article Online
View Journal | View Issue

Cite this: *Mater. Chem. Front.*, 2025, **9**, 2763

Circularly polarized room-temperature phosphorescence in microcrystals *via* aggregation-induced chirality transfer

Debin Fu, Shanting Liu and Sheng Hua Liu *

Received 22nd June 2025,
Accepted 25th July 2025

DOI: 10.1039/d5qm00447k

rsc.li/frontiers-materials

Circularly polarized room-temperature phosphorescence (CPRTP) materials integrating room-temperature phosphorescence (RTP) and circularly polarized luminescence (CPL) show great promise for frontier applications like optoelectronics. Herein, we report a chiral luminophore **Ben-2Chol**, which can self-assemble into micrometer-scale sheets in the aggregated state of solution and spin-coated films and achieve circularly polarized fluorescence (CPF) through aggregation-induced chirality transfer, with the maximum g_{lum} reaching -1.1×10^{-3}. Notably, its liquid-phase-diffused fibrous microcrystals exhibit CPRTP with inverted polarization relative to the sheets, featuring g_{lum} values of $+6.0 \times 10^{-3}$ (blue) and $+1.0 \times 10^{-3}$ (yellow-green) with a 41.7 ms of luminescence lifetime. Mechanical grinding eliminates RTP/CPL, confirming crystallization-induced properties. This study provides a simple strategy for constructing CPRTP materials through aggregation-induced chirality transfer in microcrystals, offering new insights for the design of chiral luminescent materials with dual functionalities.

Introduction

Pure organic persistent room-temperature phosphorescence (OPRTP) materials based on long-lived triplet states have garnered significant attention due to their potential applications in organic light-emitting diodes, chemical sensing, bioimaging, and information encryption.[1] Additionally, compared with transition-metal-based phosphorescent materials, OPRTP materials offer advantages such as low cost, easy synthesis, low toxicity, and superior flexibility, which are conducive to practical applications.[2] Currently, the construction of metal-free OPRTP materials typically involves introducing heavy atoms or aromatic carbonyl groups to enhance the spin–orbit coupling (SOC) effects and promote the generation of triplet excitons.[3] Meanwhile, strategies such as crystal engineering, host–guest systems, and polymer doping are employed to provide a rigid environment, thereby suppressing non-radiative decay and stabilizing triplet excitons.[4] Therefore, constructing OPRTP with long-lived triplet states under ambient atmospheric conditions remains highly challenging.

Concurrently, circularly polarized luminescence (CPL) materials have attracted extensive interest from researchers due to their potential applications in frontier scientific fields such as 3D display, chiral recognition, information encryption, and asymmetric photocatalysis.[5] The luminescence dissymmetry factor (g_{lum}) is one of the key parameters for measuring the performance of CPL materials, and practical applications require CPL materials to have a large g_{lum}.[6] However, in pure organic chiral molecular systems, it is common that chiral molecules have flexible skeletons or chiral centers that are far from the luminescent units, making such chiral luminescent molecules either hardly exhibit CPL activity or produce extremely weak CPL signals.[7] Through aggregation-driven supramolecular self-assembly, effective chiral transfer occurs, whereby chiral information is transmitted from single molecules to supramolecular levels, forming CPL-active assemblies with markedly enhanced g_{lum}.[8] On the other hand, most practical applications of CPL materials rely on aggregated states such as thin films and crystals.[9] Therefore, constructing efficient CPL aggregated-state materials is of great significance.

Circularly polarized room-temperature phosphorescence (CPRTP) materials, formed by the perfect combination of room-temperature phosphorescence (RTP) and chirality, exhibit promising application prospects in various emerging frontier fields.[10] However, current research on CPL materials primarily focuses on singlet excited states, namely, circularly polarized fluorescence (CPF). Achieving CPRTP remains challenging due to the inherent instability of triplet excitons.[11] For metal-free organic small molecules, a simple and effective strategy to realize long-lived CPRTP is a direct covalent linkage of chiral units with RTP emitters.[12] For example, in 2020, Chen *et al.* developed a pair of reversible stimuli-responsive CPRTP materials with high photo/thermal stability based on achiral

State Key Laboratory of Green Pesticide, College of Chemistry, Central China Normal University, Wuhan 430079, China. E-mail: chshliu@mail.ccnu.edu.cn

carbazole and chiral ester chains.[12a] In 2024, Li *et al.* achieved a CPRTP material by bonding chiral binaphthol with a phenoselenazine derivative, whose polystyrene thin films exhibited a high g_{lum} and long-lived CPRTP after photoactivation.[12b]

Indolo[3,2-*b*]carbazoles (ICZs) and their analogs are excellent organic semiconductor materials that have been widely applied in the field of organic optoelectronics.[13] One of the ICZ analogs, 6,12-diphenyl-5,6,11,12-tetrahydroindolo[3,2-*b*]carbazole (Ben-2H), has been reported for constructing efficient RTP materials with long triplet state lifetimes.[14] For instance, in 2019, Huang *et al.* developed a series of dual-emission OPRTP materials based on charge transfer interactions using Ben-2H as the skeleton, with lifetimes ranging from 2 to 759 ms.[14a] In 2022, Zhao *et al.* regulated the RTP and thermally activated delayed fluorescence (TADF) emissions of Ben-2H derivatives by introducing aromatic and aliphatic bromine atoms, achieving dual-persistent emissions with a long lifetime of 0.26 s and a persistent luminescence quantum yield of 10%.[14b] These findings inspired our hypothesis that introducing chiral groups into Ben-2H may help in fabricating CPRTP materials with long emission lifetimes.

As a natural chiral structure, a cholesterol unit exhibits excellent chiral stability and assembly properties, making it widely used in the development of high-performance chiral materials.[15] Herein, we synthesized a novel chiral luminophore **Ben-2Chol** by covalently linking two flexible chiral cholesterol groups to the centrosymmetric sites of a Ben-2H skeleton. The compound showed no chiral optical signals in the single-molecule state, but in the aggregated state of solution or spin-coated films, it enabled effective chiral transfer from the cholesterol side chains to the chromophore, self-assembling into micrometer-scale sheet structures and emitting CPF. Additionally, we unexpectedly obtained fibrous microcrystals of **Ben-2Chol**, which exhibited RTP with a yellow-green afterglow and a high RTP lifetime of 41.7 ms. Interestingly, compared with the micrometer-sheet aggregates, the microcrystals showed chiral optical properties with opposite polarization directions—displaying significantly enhanced CPL in the blue emission region and achieving CPRTP in the yellow-green emission region (Fig. 1).

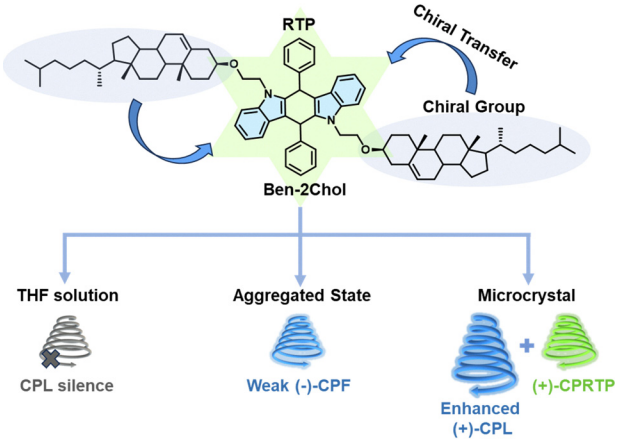

Fig. 1 Schematic of CPL of **Ben-2Chol** in various states.

Results and discussion

The target compound **Ben-2Chol** was synthesized *via* a simple one-pot nucleophilic substitution reaction of Ben-2H with Chol-Br in the presence of KOH, affording a yield of 30%. The synthetic route is described in Scheme S1. The structure of the target compound was fully characterized by ^{1}H and ^{13}C nuclear magnetic resonance (NMR) spectroscopy and high-resolution mass spectrometry (HRMS), and the results are shown in Fig. S1–S3.

The UV-vis absorption spectra and photoluminescence (PL) spectra of **Ben-2Chol** in dilute THF solution were studied (Fig. 2a). Due to the spin-allowed π–π* transition in the aromatic ring, strong absorption bands were exhibited at 264–315 nm, with a single fluorescence emission peak at 422 nm, similar to the previously reported Ben-2H.[14a] In addition, persistent luminescence of **Ben-2Chol** was observed in a THF solution at 77 K, as shown in Fig. 2b and c. After applying a gating delay time of 1 ms, the phosphorescence spectrum of **Ben-2Chol** showed dual phosphorescence emissions caused by different triplet states, with average luminescence lifetimes of 2789.5 ms and 2417.0 ms at 503 nm and 531 nm, respectively (Table S1).

In a dilute THF solution, the isolated molecules of **Ben-2Chol** showed no CD or CPL signals due to their small chiral structures and the absence of effective chiral transfer. Considering that alkyl chains facilitate molecular self-assembly, we promoted the self-assembly of **Ben-2Chol** by adding water as a poor solvent, aiming to achieve amplified chirality. The fluorescence spectra of **Ben-2Chol** in THF/water mixtures with different water fractions (f_w) are shown in Fig. 2d. With an increase in the water content, the fluorescence intensity showed an increasing trend, reaching its peak when f_w reached 60% (Fig. 2e). The fluorescence quantum efficiency increased from 39.9% (THF solution) to 45.8% (f_w = 60%), indicating that **Ben-2Chol** exhibited typical aggregation-induced emission enhancement (AIEE) characteristics in the THF/water mixed system (Table S2).

We further measured the CD signals of **Ben-2Chol** at different f_w (Fig. 2f and Fig. S5). A weak positive CD peak emerged at 303 nm when the f_w reached 40%. As the f_w increased to 60%, a significantly enhanced negative CD signal appeared at approximately 243 nm. Upon further increasing f_w to 70%, the negative CD peak exhibited a slight intensification and blue-shifted to 233 nm, accompanied by the emergence of a positive CD signal at 245 nm. Correspondingly, in Fig. 2f, the absorption peak underwent distinct shape changes with increasing water content, accompanied by a notable tailing effect in the visible light region, which was attributed to the light scattering caused by nanoparticle formation.[16] Using CPL spectroscopy, we probed the excited-state chirality of the aggregated solutions. Weak negative CPF signals were detected in the aggregated states at f_w of 60% and 70%, with fluorescence lifetimes of 6.1 ns and 6.2 ns, and g_{lum} values of -4.8×10^{-4}

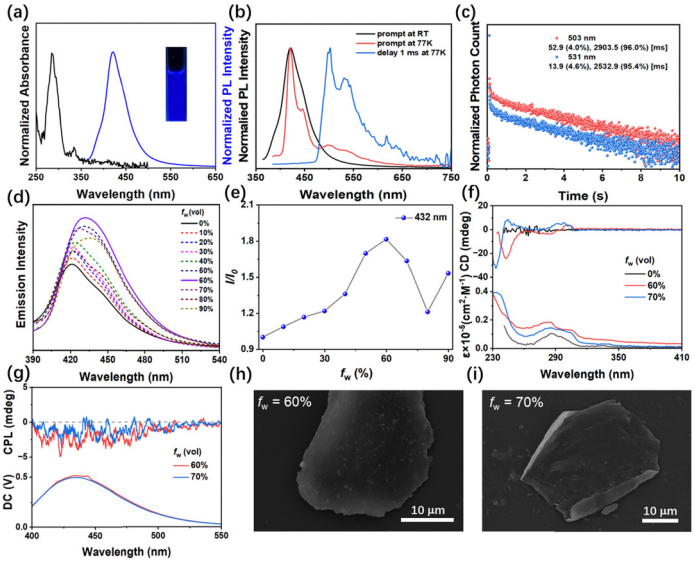

Fig. 2 (a) UV-vis absorption (black line) and PL (blue line) spectra of **Ben-2Chol** (excitation wavelength = 340 nm) in THF at 293 K. Inset: Photographs taken under a 365 nm UV radiation. (b) Normalized steady-state (293 K, black line; 77 K, red line) and delayed (77 K, blue line) emission spectra of **Ben-2Chol** (excitation wavelength = 340 nm) in THF. (c) Lifetime decay profiles of **Ben-2Chol** (excitation wavelength = 340 nm) in THF at 77 K. (d) Fluorescence spectra of **Ben-2Chol** (excitation wavelength = 340 nm) in THF/water mixed solvents. (e) Plot of the relative emission peak intensity *versus* f_w at 432 nm for the THF/water mixed solvents, where I = emission intensity and I_0 = emission intensity in the THF solution. (f) CD spectra and (g) CPL spectra of **Ben-2Chol** (excitation wavelength = 300 nm) in THF/water mixed solvents with various f_w values. SEM images of the assemblies formed by **Ben-2Chol** in THF/H_2O mixed solvents with (h) f_w = 60% and (i) f_w = 70%. Concentration: 1.0 × 10^{-5} mol L^{-1}.

and -2.3×10^{-4}, respectively (Fig. 2g and Fig. S4, S6). These results demonstrate that aggregation induces the transfer of chirality from the chiral carbon center to the chromophore, thereby enhancing the chiroptical activity of the molecules. In addition, the morphology of the aggregates in solution was visualized by scanning electron microscopy (SEM) (Fig. 2h, i and Fig. S7). The SEM images revealed that **Ben-2Chol** molecules self-assembled into two-dimensional (2D) thin sheets with sizes of tens of micrometers. The sheet-like aggregates presented a planar morphology, with the lateral dimensions ranging from tens to hundreds of micrometers and a relatively uniform thickness, indicating that there was a high degree of structural order during the self-assembly process, which facilitated the realization of chirality amplification from single molecules to supramolecules.

By manipulating the volume ratio of the THF/water mixed solvent, the above-mentioned chiral amplification preliminarily demonstrated its characteristic of chiral transfer through aggregation induction. We further prepared PMMA-doped films and pure films of **Ben-2Chol** to study their chiral optical properties in the thin-film state. Compared with the PMMA-doped films, the pure film exhibited a slight red-shift in its emission peak, while the PMMA-doped films showed emission characteristics similar to those in the THF solution state (Fig. 3a). In addition, both films showed fluorescent emission. The PMMA-doped films (8.3 ns) exhibited a longer luminescence lifetime than the pure film (3.0 ns) and a higher fluorescence quantum yield (Table S2 and Fig. S8).

As expected, when the doping concentration of **Ben-2Chol** in the PMMA films was 0.1 wt%, its CD signal was too weak to be noticeable. However, when the concentration was increased to 1.0 wt%, two enhanced negative CD signals were observed at 326 nm and 251 nm. Similarly, the pure films exhibited negative CD signals at 247 nm and 344 nm, with intensities comparable to those of the PMMA film at high doping concentrations (Fig. 3b). Notably, the CPF signal of the pure films showed a significantly enhanced negative signal compared with that of the aggregated state in solution, with the g_{lum} value

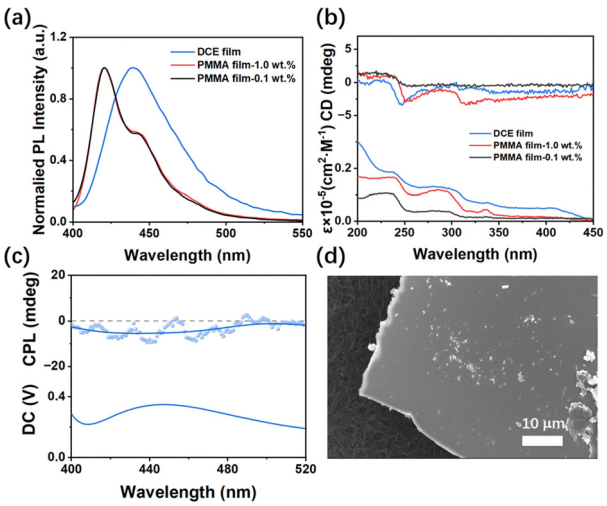

Fig. 3 (a) PL spectra and (b) CD spectra of the PMMA films doped with **Ben-2Chol** (0.1 wt%, black line; 1.0 wt%, red line) and the neat film of **Ben-2Chol** (the film was prepared from a **Ben-2Chol** DCE solution with a concentration of 10 mg mL^{-1}, blue line). (c) CPL spectra (excitation wavelength = 300 nm) and (d) SEM image of the neat film of **Ben-2Chol**.

reaching -1.1×10^{-3} (Fig. 3c and Fig. S9). SEM observations revealed the formation of self-assembled micrometer-scale sheet structures in the films, which were highly similar to the nanosheet structures in the solution-aggregated state (Fig. 3d and Fig. S10). However, the higher degree of molecular aggregation in the film state led to a significant enhancement of the CPF signal. These results fully demonstrated that the molecular aggregation behavior in the **Ben-2Chol** system played a crucial role in the amplification of the chiral optical signals.

We slowly added ethanol to a concentrated dichloromethane solution of **Ben-2Chol** and obtained a microcrystalline sample with RTP property through liquid-phase diffusion. As shown in the SEM image of Fig. 4a and Fig. S11, the microcrystals exhibited regular elongated fibrous structures, with lengths ranging from tens to hundreds of micrometers, which were significantly different from the plate-like structures of the solution-aggregated state and pure films. Additionally, powder X-ray diffraction (XRD) results showed sharp diffraction peaks of the microcrystals, confirming their crystalline phase structure (Fig. 4b).

The phosphorescence properties of **Ben-2Chol** microcrystals were further studied by PL spectroscopy (Fig. 4c and Table S3). At room temperature, the maximum emission peak of the microcrystals was located at 431 nm with an emission lifetime of 4.4 ns, exhibiting a blue light emission. After applying a 1 ms delay time-gated technique, the phosphorescence spectrum showed dual phosphorescence emissions at 439 nm and 541 nm. At 77 K, the maximum emission peak was located at 425 nm, with an emission lifetime of 1.8 ns; this peak was slightly blue-shifted compared to room temperature, and the relative intensity ratio of emissions in the blue and yellow-green spectral regions decreased. Using the 1 ms delay time-gated technique, the phosphorescence spectrum showed a broad emission peak with the maximum emission at 497 nm across the 400–700 nm range. The room-temperature phosphorescence lifetimes of the microcrystals at 439 nm and 541 nm were 15.2 ms and 41.7 ms, respectively (Fig. 4d and Fig. S13). Significantly prolonged phosphorescence lifetimes were observed at 77 K with the phosphorescence lifetime at 497 nm reaching up to 222.9 ms (Fig. S14). It was worth noting that the blue-emission region exhibited both nanosecond and millisecond luminescence lifetimes, indicating that the emission in the blue light portion was composed of both fluorescence and phosphorescence.

Under excitation with a 365 nm ultraviolet lamp at room temperature, **Ben-2Chol** microcrystals exhibited bright blue light emission. Due to the presence of components with long emission lifetimes, a yellow-green afterglow lasting approximately 2.5 s was observed after turning off the UV lamp. Interestingly, this afterglow emission disappeared after mechanical grinding (Fig. 4e). PL spectroscopy revealed a slight blue-shift in the emission peak after grinding, with no obvious change in the peak profile (Fig. S15). However, the long-lived component vanished, and the ground sample exhibited nanosecond-scale fluorescence emission with a lifetime of 3.2 ns (Table S2 and Fig. S16). SEM images showed that the crystalline fibers disappeared after intense grinding, with the morphology transforming into disordered bulk structures (Fig. S17). XRD patterns also indicated that the ground sample lacked any sharp diffraction signals, confirming its amorphous (non-crystalline) state (Fig. 4b). These results indicated that the RTP phenomenon of **Ben-2Chol** was crystallization-induced. The underlying mechanism might be related to the facts that the weak intermolecular interactions in the crystal promoted charge transfer between molecules

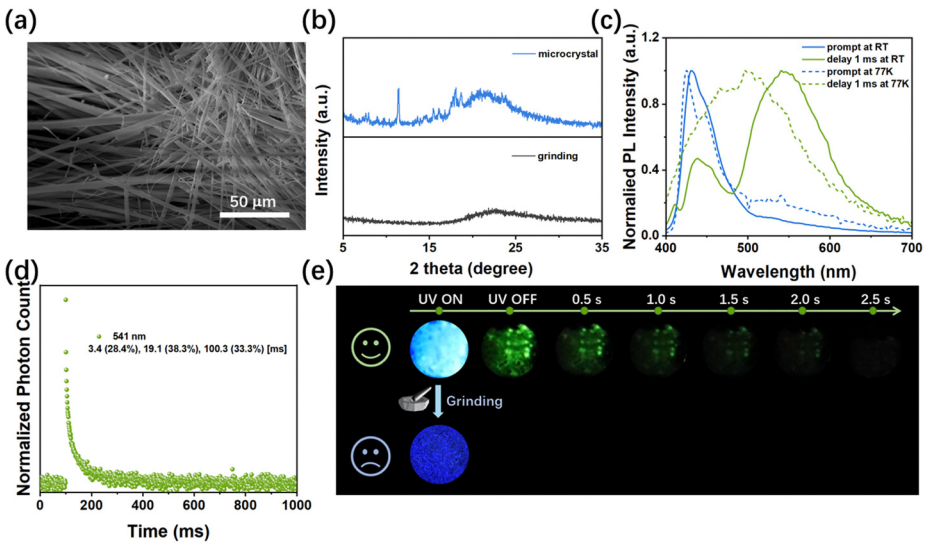

Fig. 4 (a) SEM image of **Ben-2Chol** in microcrystalline state. (b) XRD patterns of **Ben-2Chol** in microcrystalline state before (blue line) and after (black line) grinding. (c) Normalized steady-state (293 K, blue solid line; 77 K, blue dashed line) and delayed (77 K, green solid line; 77 K, green dashed line) emission spectra of **Ben-2Chol** (excitation wavelength = 340 nm) in microcrystalline state. (d) Lifetime decay profile of **Ben-2Chol** in microcrystalline state at 541 nm under room temperature. (e) Luminescence photographs of **Ben-2Chol** in microcrystalline state and amorphous state before and after a 365 nm UV excitation.

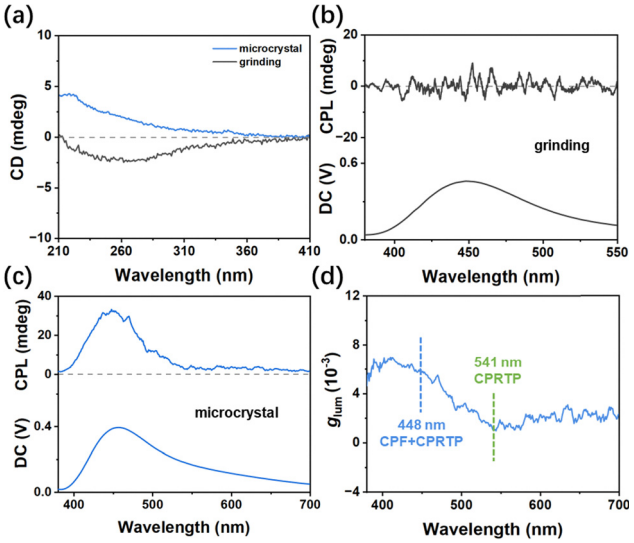

Fig. 5 (a) CD spectra of **Ben-2Chol** microcrystals before (blue line) and after (black line) grinding. CPL spectra (excitation wavelength = 300 nm) of **Ben-2Chol** microcrystals (b) after and (c) before grinding. (d) g_{lum} spectra of **Ben-2Chol** microcrystals.

and the rigid environment stabilized the triplet excited state.[14a]

Further studies on the chiral properties of **Ben-2Chol** microcrystals were conducted. The CD spectrum showed that the microcrystals exhibited positive CD signals in the range of 210–400 nm (Fig. 5a). As shown in Fig. 5c of the CPL spectrum, the microcrystals displayed a significantly stronger positive CPL signal in the range of 380–500 nm, and the CPL emission was extended all the way to 700 nm. Based on the RTP emission property of the microcrystals, it was proposed that both CPF and CPRTP coexisted in the blue emission region, while the weaker signals at longer wavelengths were ascribed to CPRTP.[17] The g_{lum} values at 448 nm and 541 nm were $+6.0 \times 10^{-3}$ and $+1.0 \times 10^{-3}$, respectively (Fig. 5d). Interestingly, the microcrystals exhibited a supramolecular chirality that was completely different from other aggregates, with opposite chiral information in the ground state and excited state and significantly enhanced CPL emission. Notably, after mechanical grinding, the CD signal of the microcrystals weakened and reversed, and no CPL emission was detected (Fig. 5a, b and Fig. S18). These results indicated that the CPRTP of **Ben-2Chol** microcrystals were dependent on the rigid environment of the crystalline phase, which significantly stabilized triplet excitons. This characteristic enabled the CPRTP of the microcrystals to respond to mechanical stimuli.

Conclusions

In summary, we synthesized a novel chiral luminophore **Ben-2Chol**, which exhibited no chiroptical signals in dilute THF solution but self-assembles into micrometer-scale sheet structures in aggregated states, enabling aggregation-induced chirality transfer and CPF. Notably, the fibrous microcrystals of **Ben-2Chol** prepared *via* a liquid-phase diffusion displayed CPRTP with the polarization directions opposite to those of the aggregated sheets, featuring g_{lum} values of $+6.0 \times 10^{-3}$ (blue region) and $+1.0 \times 10^{-3}$ (yellow-green region), along with an RTP lifetime of 41.7 ms at 541 nm. Mechanical grinding disrupted the crystalline structure, eliminating both the RTP and CPL signals, confirming the crystallization-induced nature of CPRTP. This study presents a simple strategy for constructing CPRTP materials through aggregation-induced chirality transfer, offering new insights for the design of chiral luminescent materials with dual RTP and CPL functionalities.

Conflicts of interest

There are no conflicts to declare.

Data availability

All supporting data are included in the article and its SI.

Detailed experimental sections, NMR spectroscopy, and comprehensive information on thin film preparation. See DOI: https://doi.org/10.1039/d5qm00447k

Acknowledgements

We acknowledge financial support from the National Natural Science Foundation of China (22175069), and the Fundamental Research Funds for the Central Universities (CCNU25ZZ281). The authors gratefully acknowledge the technical contributions of Dr. Zhengping Fang with structural analysis and characterization.

Notes and references

1 (*a*) D. Cui, L. Zhang, J. Zhang, W. Li, J. Chen, Z. Guo, C. Sun, Y. Wang, W. Wang, S. Li, W. Huang, C. Zheng and R. Chen, Hybrid local and charge-transfer material with ultralong room temperature phosphorescence for efficient organic afterglow light-emitting diodes, *Angew. Chem., Int. Ed.*, 2024, **63**, e202411588; (*b*) Q. Wu, H. Ma, K. Ling, N. Gan, Z. Cheng, L. Gu, S. Cai, Z. An, H. Shi and W. Huang, Reversible ultralong organic phosphorescence for visual and selective chloroform detection, *ACS Appl. Mater. Interfaces*, 2018, **10**, 33730–33736; (*c*) Y. Fan, S. Liu, M. Wu, L. Xiao, Y. Fan, M. Han, K. Chang, Y. Zhang, X. Zhen, Q. Li and Z. Li, Mobile phone flashlight-excited red afterglow bioimaging, *Adv. Mater.*, 2022, **34**, 2201280; (*d*) W. Li, Q. Huang, Z. Mao, X. He, D. Ma, J. Zhao, J. W. Y. Lam, Y. Zhang, B. Z. Tang and Z. Chi, A dish-like molecular architecture for dynamic ultralong room-temperature phosphorescence through reversible guest accommodation, *Nat. Commun.*, 2022, **13**, 7423; (*e*) W. Zhao, Z. He and B. Z. Tang, Room-temperature phosphorescence from organic aggregates, *Nat. Rev. Mater.*, 2020, **5**, 869–885; (*f*) S. Cai, X. Yao, H. Ma, H. Shi and Z. An, Manipulating

intermolecular interactions for ultralong organic phosphorescence, *Aggregate*, 2023, **4**, e320; (*g*) Y. Gao, W. Yuan, Y. Li, A. Huang, Y. Fang, A. Li, K. Wang, B. Zou, Q. Li and Z. Li, Accurately adjusted phenothiazine conformations: reversible conformation transformation at room temperature and self-recoverable stimuli-responsive phosphorescence, *Light: Sci. Appl.*, 2025, **14**, 99; (*h*) Q. Zhang, Y. Fan, Q. Liao, C. Zhong, Q. Li and Z. Li, Room temperature phosphorescence achieved by aromatic/perfluoroaromatic interactions, *Sci. China: Chem.*, 2022, **65**, 918.

2 (*a*) Y. Li, M. Gecevicius and J. Qiu, Long persistent phosphors—from fundamentals to applications, *Chem. Soc. Rev.*, 2016, **45**, 2090–2136; (*b*) S. Xu, R. Chen, C. Zheng and W. Huang, Excited state modulation for organic afterglow: materials and applications, *Adv. Mater.*, 2016, **28**, 9920–9940; (*c*) Z.-H. Zhao, P.-C. Zhao, S.-Y. Chen, Y.-X. Zheng, J.-L. Zuo and C.-H. Li, Tough, reprocessable, and recyclable dynamic covalent polymers with ultrastable long-lived room-temperature phosphorescence, *Angew. Chem., Int. Ed.*, 2023, **62**, e202301993.

3 (*a*) Z. Cong, M. Han, Y. Fan, Y. Fan, K. Chang, L. Xiao, Y. Zhang, X. Zhen, Q. Li and Z. Li, Ultralong blue room-temperature phosphorescence by cycloalkyl engineering, *Mater. Chem. Front.*, 2022, **6**, 1606–1614; (*b*) T. Zhu, T. Yang, Q. Zhang and W. Z. Yuan, Clustering and halogen effects enabled red/near-infrared room temperature phosphorescence from aliphatic cyclic imides, *Nat. Commun.*, 2022, **13**, 2658; (*c*) D. Zhong, S. Liu, L. Yue, Z. Feng, H. Wang, P. Yang, B. Su, X. Yang, Y. Sun and G. Zhou, Achieving pure room temperature phosphorescence (RTP) in phenoselenazine-based organic emitters through synergism among heavy atom effect, enhanced n → π* transitions and magnified electron coupling by the A–D–A molecular configuration, *Chem. Sci.*, 2024, **15**, 9112–9119; (*d*) G. Xie, N. Guo, X. Xue, Q. Yang, X. Liu, H. Li, H. Li, Y. Tao, R. Chen and W. Huang, Resonance-induced dynamic triplet exciton population for photoactivated organic ultralong room temperature phosphorescence, *J. Am. Chem. Soc.*, 2024, **146**, 20449–20457.

4 (*a*) Y. Zheng, Z. Wang, J. Liu, Y. Zhang, L. Gao, C. Wang, X. Zheng, Q. Zhou, Y. Yang, Y. Li, H. Tang, L. Qu, Y. Zhao and C. Yang, Long-lived room temperature phosphorescence crystals with green light excitation, *ACS Appl. Mater. Interfaces*, 2022, **14**, 15706–15715; (*b*) B. Ding, X. Ma and H. Tian, Recent advances of pure organic room temperature phosphorescence based on functional polymers, *Acc. Mater. Res.*, 2023, **4**, 827–838; (*c*) S. Li, J. Gu, J. Wang, W. Yuan, G. Ye, L. Yuan, Q. Liao, L. Wang, Z. Li and Q. Li, Excellent persistent near-infrared room temperature phosphorescence from highly efficient host–guest systems, *Adv. Sci.*, 2024, **11**, 2402846; (*d*) Y. Gao, J. Lu, Q. Liao, S. Li, Q. Li and Z. Li, Thermal annealing promoted room temperature phosphorescence: motion models and internal mechanism, *Natl. Sci. Rev.*, 2023, **10**, nwad239.

5 (*a*) Y. Zhou, Y. Wang, Y. Song, S. Zhao, M. Zhang, G. Li, Q. Guo, Z. Tong, Z. Li, S. Jin, H.-B. Yao, M. Zhu and T. Zhuang, Helical-caging enables single-emitted large asymmetric full-color circularly polarized luminescence, *Nat. Commun.*, 2024, **15**, 251; (*b*) Y. Zhu, T. Ding, X. Zhang, Y. Zhou, J. Yu, X. Li, H. Zheng, Z. Sun and C. Jiao, Noncovalent induced circular dichroism sensors based on a chiral metal–organic framework: chiral induction synthesis, quantitative enantioselective sensing and noncovalent sensing mechanism, *Inorg. Chem. Front.*, 2023, **10**, 2818–2828; (*c*) S. Lin, Y. Tang, W. Kang, H. K. Bisoyi, J. Guo and Q. Li, Photo-triggered full-color circularly polarized luminescence based on photonic capsules for multilevel information encryption, *Nat. Commun.*, 2023, **14**, 3005; (*d*) C. He, G. Yang, Y. Kuai, S. Shan, L. Yang, J. Hu, D. Zhang, Q. Zhang and G. Zou, Dissymmetry enhancement in enantioselective synthesis of helical polydiacetylene by application of superchiral light, *Nat. Commun.*, 2018, **9**, 5117; (*e*) T. Li, X. Zhu, G. Ouyang and M. Liu, Circularly polarized luminescence from chiral macrocycles and their supramolecular assemblies, *Mater. Chem. Front.*, 2023, **7**, 3879–3903; (*f*) X. Yang, X. Lin, Y. Zhao, Y. S. Zhao and D. Yan, Lanthanide metal–organic framework microrods: colored optical waveguides and chiral polarized emission, *Angew. Chem., Int. Ed.*, 2017, **56**, 7853.

6 M.-J. Ji, W.-L. Zhao, M. Li and C.-F. Chen, Circularly polarized luminescence with high dissymmetry factors for achiral organic molecules in solutions, *Nat. Commun.*, 2025, **16**, 2940.

7 B.-H. Liu, Y. Zong, N. Liu and Z.-Q. Wu, Advances in self-assembly-based circularly polarized luminescent materials, *Sci. China: Chem.*, 2024, **67**, 3247–3257.

8 (*a*) Y. Sang, J. Han, T. Zhao, P. Duan and M. Liu, Circularly polarized luminescence in nanoassemblies: generation, amplification, and application, *Adv. Mater.*, 2020, **32**, 1900110; (*b*) Z.-L. Gong, T.-X. Dan, J.-C. Chen, Z.-Q. Li, J. Yao and Y.-W. Zhong, Boost the circularly polarized phosphorescence of chiral organometallic platinum complexes by hierarchical assembly into fibrillar networks, *Angew. Chem., Int. Ed.*, 2024, **63**, e202402882.

9 (*a*) G. Albano, G. Pescitelli and L. D. Bari, Chiroptical properties in thin films of π-conjugated systems, *Chem. Rev.*, 2020, **120**, 10145–10243; (*b*) J. Han, Y. Shi, X. Jin, X. Yang and P. Duan, Regulating the excited state chirality to fabricate high-performance-solid-state circularly polarized luminescence materials, *Chem. Sci.*, 2022, **13**, 6074–6080; (*c*) Q. Liao, Q. Li and Z. Li, The key role of molecular packing in luminescence property: from adjacent molecules to molecular aggregates, *Adv. Mater.*, 2023, **35**, 2306617.

10 (*a*) J. Song, H. Xiao, L. Fang, L. Qu, X. Zhou, Z.-X. Xu, C. Yang and H. Xiang, Highly phosphorescent planar chirality by bridging two square-planar platinum(II) complexes: chirality induction and circularly polarized luminescence, *J. Am. Chem. Soc.*, 2022, **144**, 2233–2244; (*b*) D. Liu, W.-J. Wang, P. Alam, Z. Yang, K. Wu, L. Zhu, Y. Xiong, S. Chang, Y. Liu, B. Wu, Q. Wu, Z. Qiu, Z. Zhao and B. Z. Tang, Highly efficient circularly polarized near-infrared phosphorescence

in both solution and aggregate, *Nat. Photonics*, 2024, **18**, 1276–1284; (*c*) J. You, C. Yin, S. Wang, X. Wang, K. Jin, Y. Wang, J. Wang, L. Liu, J. Zhang and J. Zhang, Responsive circularly polarized ultralong room temperature phosphorescence materials with easy-to-scale and chiral-sensing performance, *Nat. Commun.*, 2024, **15**, 7149; (*d*) M. Cao, Y. Ren, Y. Wu, J. Shen, S. Li, Z.-Q. Yu, S. Liu, J. Li, O. J. Rojas and Z. Chen, Biobased and biodegradable films exhibiting circularly polarized room temperature phosphorescence, *Nat. Commun.*, 2024, **15**, 2375; (*e*) X. Wang, S. Ma, B. Zhao and J. Deng, Frontiers in circularly polarized phosphorescent materials, *Adv. Funct. Mater.*, 2023, **33**, 2214364.

11 M. Xu, X. Wu, Y. Yang, C. Ma, W. Li, H. Yu, Z. Chen, J. Li, K. Zhang and S. Liu, Designing hybrid chiral photonic films with circularly polarized room-temperature phosphorescence, *ACS Nano*, 2020, **14**, 11130–11139.

12 (*a*) H. Li, H. Li, W. Wang, Y. Tao, S. Wang, Q. Yang, Y. Jiang, C. Zheng, W. Huang and R. Chen, Stimuli-responsive circularly polarized organic ultralong room temperature phosphorescence, *Angew. Chem., Int. Ed.*, 2020, **59**, 4756–4762; (*b*) S. Fu, Y. Chen, Y. Xie and Z. Li, Photoactivated circularly polarized room-temperature phosphorescence from phenoselenazine derivative and its application in information security, *Chin. J. Chem.*, 2024, **42**, 2499–2506; (*c*) L. Yu, Z. Gao, H. Cheng, X. Yan, H. Cao, G. Guo, H. Li, P. Li, R. Chen and Y. Tao, Time-dependent colorful circularly polarized organic ultralong room temperature phosphorescence from a single-component chiral molecule, *Small*, 2023, **19**, 2303579; (*d*) Y. Yang, S. Xiao, Y. Zhou, C. Shi, L. Xu, X. Liao, N. Su, N. Sun, Y.-X. Zheng, L. Ding and J. Ding, Chiral perturbation in D-O-A organic phosphors towards efficient circularly polarized electroluminescence, *Sci. China Mater.*, 2024, **68**, 1351–1358.

13 (*a*) H. Jiang, H. Zhao, K. K. Zhang, X. Chen, C. Kloc and W. Hu, High-performance organic single-crystal field-effect transistors of indolo[3,2-b]carbazole and their potential applications in gas controlled organic memory devices, *Adv. Mater.*, 2011, **23**, 5075–5080; (*b*) G. Zhao, H. Dong, Q. Liao, J. Jiang, Y. Luo, H. Fu and W. Hu, Organic field-effect optical waveguides, *Nat. Commun.*, 2018, **9**, 4790; (*c*) E. Jatautiene, J. Simokaitiene, G. Sych, D. Volyniuk, K. Ivaniuk, P. Stakhira, V. Fitio, H. Petrovska, V. Savaryn, Y. Nastishin and J. V. Grazulevicius, Adjustment of electronic and emissive properties of indolocarbazoles for non-doped OLEDs and cholesteric liquid crystal lasers, *Appl. Mater. Today*, 2021, **24**, 101121; (*d*) R. Chowdhury, M. D. Preuss, H.-H. Cho, J. J. P. Thompson, S. Sen, T. K. Baikie, P. Ghosh, Y. Boeije, X. W. Chua, K.-W. Chang, E. Guo, J. V. D. Tol, B. W. L. V. D. Bersselaar, A. Taddeucci, N. Daub, D. M. Dekker, S. T. Keene, G. Vantomme, B. Ehrler, S. C. J. Meskers, A. Rao, B. Monserrat, E. W. Meijer and R. H. Friend, Circularly polarized electroluminescence from chiral supramolecular semiconductor thin films, *Science*, 2025, **387**, 1175–1181.

14 (*a*) F. Li, S. Guo, Y. Qin, Y. Shi, M. Han, Z. An, S. Liu, Q. Zhao and W. Huang, Achieving dual persistent room-temperature phosphorescence from polycyclic luminophores via inter-/intramolecular charge transfer, *Adv. Opt. Mater.*, 2019, **7**, 1900511; (*b*) F. Li, C. Qian, J. Lu, Y. Ma, K. Y. Zhang, S. Liu and Q. Zhao, Color-tunable dual persistent emission via a triplet exciton reservoir for temperature sensing and anti-counterfeiting, *Adv. Opt. Mater.*, 2022, **10**, 2101773.

15 (*a*) Q. Xia, L. Meng, T. He, G. Huang, B. S. Li and B. Z. Tang, Direct visualization of chiral amplification of chiral aggregation induced emission molecules in nematic liquid crystals, *ACS Nano*, 2021, **15**, 4956–4966; (*b*) Y. Wu, C. Yan, X.-S. Li, L. H. You, Z.-Q. Yu, X. Wu, Z. Zheng, G. Liu, Z. Guo, H. Tian and W.-H. Zhu, Circularly polarized fluorescence resonance energy transfer (C-FRET) for efficient chirality transmission within an intermolecular system, *Angew. Chem., Int. Ed.*, 2021, **60**, 24549–24557; (*c*) K. Fu, Y. Zhao and G. Liu, Pathway-directed recyclable chirality inversion of coordinated supramolecular polymers, *Nat. Commun.*, 2024, **15**, 9571; (*d*) H. Zhang, X. Chang, C. Ma, G. Huang, B. S. Li and B. Z. Tang, Two cholesterol-containing pyrene derivatives: subtle spacer difference, diverse stimuli-responsive luminescence, chirality, and self-assembly behaviors, *ACS Appl. Mater. Interfaces*, 2022, **14**, 43926–43936; (*e*) J. Zhang, A. Hao and P. Xing, Oxidation triggered supramolecular chirality, *Nano Lett.*, 2024, **24**, 16191–16199.

16 H. Auweter, H. Haberkorn, W. Heckmann, D. Horn, E. Lüddecke, J. Rieger and H. Weiss, Supramolecular structure of precipitated nanosize beta-carotene particles, *Angew. Chem., Int. Ed.*, 1999, **38**, 2188–2191.

17 X. Nie, Y. Zhang, B. Wu, Z. Ye, F. Gao, Y. Chen, C. Wang, D. Zhu, P. Alam, Z. Qiu and B. Z. Tang, Dynamic chirality in nature-inspired photonic crystal films: ultralong room temperature phosphorescence and stimuli-responsive circularly polarized luminescence, *ACS Nano*, 2025, **19**, 11221–11229.